

<https://doi.org/10.1038/s42005-025-02000-9>

Photonic spiking neural network built with a single VCSEL for high-speed time series prediction

Check for updates

Dafydd Owen-Newns¹ ✉, Lina Jaurigue², Joshua Robertson¹, Andrew Adair¹,
Jonnel Anthony Jaurigue², Kathy Lüdge² & Antonio Hurtado¹

Photonic technologies hold significant potential for creating innovative, high-speed, efficient and hardware-friendly neuromorphic computing platforms. Neuromorphic photonic methods leveraging ubiquitous, technologically mature and cost-effective Vertical-Cavity Surface Emitting Lasers (VCSELs) are of notable interest. VCSELs have demonstrated the capability to replicate neuronal optical spiking responses at ultrafast rates. Previously, a photonic Spiking Neural Network (p-SNN) using a single VCSEL has been demonstrated for use in classification tasks. Here, it is applied to a more complex time-series prediction task. The VCSEL p-SNN combined with a technique to induce network memory, is applied to perform multi-step-ahead predictions of a chaotic time-series. By providing the feedforward p-SNN with only two temporally separated inputs excellent accuracy is experimentally demonstrated over a range of prediction horizons. VCSEL-based p-SNNs therefore offer ultrafast, efficient operation in complex predictive tasks whilst enabling hardware implementations. The inherent attributes and performance of VCSEL p-SNNs hold great promise for use in future light-enabled neuromorphic computing hardware.

Artificial Neural Networks (ANNs) form a core component of many implementations of Artificial Intelligence (AI) due to their demonstrated capability to deliver high-level performance in various complex information processing tasks like pattern recognition, data classification, and image and language processing. ANNs are inspired by the functioning of biological neurons in the brain, consisting of parallel arrays of large numbers of nodes (neurons) that use non-linear transformations to achieve efficient processing and decision-making. Neuromorphic (brain-like) processing aims at reproducing and exploiting the spike-based signalling in biological neurons for computation and has gathered extensive research interest in recent years. Driven by the desire to find novel computing architectures not limited by the challenges of traditional digital computing platforms, research into neuromorphic processing has led to spike-operating electronic processing systems such as Loihi 2¹, TrueNorth², Spinnaker 2³ and BrainScaleS-2⁴ (see ref. 5 for a review).

Photonic systems, offer further avenues of development in neuromorphic computing⁶ that make use of the fundamental advantages intrinsic to the optical medium (e.g. high bandwidth, reduced cross-talk, long communication links, etc.) and that can help overcome inherent limitations arising in electronic-based platforms. Optical devices offer high data throughput due to the capability to transmit many signals in the same

channel without interference, granting high computation densities and parallelism via wavelength and mode multiplexing techniques. Additionally, photonics has access to a range of linear and nonlinear interactions that can be implemented with high efficiency and leveraged for information processing functionalities. Furthermore, photonics offers prospects for the implementation of low power data links, with faster baseline operating speeds, for a promising highly energy efficient neuromorphic computing platform. The realisation of such neural networks using photonic technologies have been shown recently using a number of systems such as optical modulators⁷, micro-ring weight banks⁸, phase change materials⁹ and semiconductor lasers^{10,11}. Semiconductor lasers are of particular interest due to their dynamical behaviour, which allow for the implementation of neuronal-like responses at ultrafast speeds. In particular, one type of semiconductor laser, the Vertical-Cavity Surface-Emitting Laser (VCSEL) has been the subject of extensive research as it has been demonstrated to exhibit spiking dynamics similar to those of biological neurons but at ultrafast sub-nanosecond speeds.

VCSELs are industrially ubiquitous semiconductor lasers, found in a wide variety of consumer devices (e.g. mobile phones, automotive sensors), as well as in telecommunications and data centres. Interestingly, VCSELs operating in the 1310 and 1550 nm telecom windows have demonstrated

¹Institute of Photonics, SUPA Department of Physics, University of Strathclyde, 99 George Street, G1 1RD Glasgow, UK. ²Technische Universität Ilmenau, Institut für Physik, Weimarer Straße 25, 98693 Ilmenau, Germany. ✉e-mail: dafydd.owen-newns@strath.ac.uk

excitable neuronal behaviours, emitting controllable optical spikes in response to optical signals injected into the laser cavity¹². The neural-like optical spikes produced by VCSEs are short (~100ps-long) and can be triggered at rates up to a few GHz. They also exhibit other useful neuro-morphic properties such as spike-firing thresholding, integration-and-fire responses and refractoriness^{13–15}. These properties have been used for several purposes: implementing logical XOR operation¹⁶; and image processing tasks ranging from pattern recognition^{17–19} to rate-coding²⁰. Due to the maturity of VCSEL technology, this increasingly promising approach to photonic artificial spiking neurons can be realised with off-the-shelf optical components at key telecom wavelengths and in hardware-friendly configurations, helping remove the barrier of expensive bespoke designs.

One established use of VCSEs for ANNs is in photonic-based reservoir computing (RC). These are large scale, recurrent neural networks in which all internal connections and input layer weights are fixed, and only the output layer weights require training. Photonic RC systems have demonstrated good performance in several complex tasks, and as the parameters and connectivity of the reservoir are fixed, they are ideal to implement in purpose-built photonic hardware. Photonic RC systems have been implemented in recent years using optoelectronic and a wide range of optical devices^{21–26}, including micro-ring resonators, photonic integrated systems and semiconductor lasers. In particular, VCSEL-based photonic RC systems, have attracted important research attention due to their dual linear polarisation emission and lower energy operation, which can be leveraged to improve computing performance^{27,28}. VCSEL photonic RC systems have been constructed using space-^{29,30} and time-multiplexing^{31,32} paradigms, in which the nodes and connections of the network are defined by the time varying (or spatial) dynamics of light in the laser cavity (see ref. 33 for a review of VCSEL-based approaches to RC).

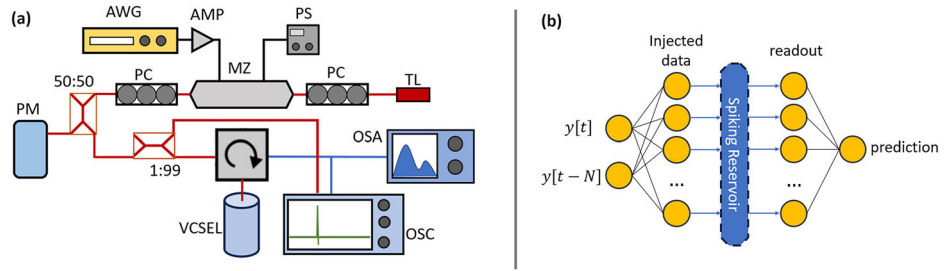
Recently, the optical spiking dynamics exhibited by VCSEs have been utilised in combination with time-multiplexing techniques to construct a photonic Spiking Neural Network (p-SNN)³⁴. This p-SNN was built with a single time-multiplexed VCSEL, the network connections and the nonlinear transformation were provided by the excitable optical spiking dynamics of the device. These link information between many network nodes for effective data processing, demonstrating excellent performance on classification tasks, as they enable separating data with complex decision boundaries. Importantly, the use of optical spiking signals to process information offers key benefits when compared to traditional non-spiking photonic neural network implementations. These include the possibility to use novel training algorithms that only require the training of very few network nodes (increasing training simplicity and overall processing speed), they allow operation with sparse signalling and weight matrices, and they can perform accurately even when low dataset sizes are used for training³⁵.

However, to date these p-SNNs lack internal memory and cannot therefore operate in key tasks, such as time-series prediction, which are of strategic importance in a variety of sectors (e.g. predictive maintenance, weather forecasting, etc.). This work tackles this fundamental challenge by demonstrating the successful operation of a p-SNN built with a single, commercially-sourced, telecom-wavelength VCSEL on a chaotic timeseries prediction task. Specifically, we demonstrate experimentally the p-SNN's successful execution of multi-step-ahead prediction of the chaotic Mackey-Glass time series. This task requires that the system produces an output corresponding to a real number (the time-series value), and that the system has knowledge of previous temporal data inputs (memory). This requires going beyond the simpler operation in classification tasks for which memory is not required and whose output is limited to an element of a finite set (equal to the number of datapoint classes). Here, we demonstrate the successful performance of the p-SNN overcoming these fundamental challenges caused by the representation of real numbers with discrete neural-like spikes, and the lack of (memory enhancing) feedback network connections. We achieve this by applying a memory-inducing technique in the pre-processing of the input data that has recently been shown to be an effective means of improving the performance of reservoir computers on tasks requiring memory^{36,37}.

The p-SNN created in this work deploys concepts from spiking and time-multiplexed neural networks as well as from the Reservoir Computing (RC) paradigm. Unlike standard neural network approaches that implement in hardware many (spatial) nodes and network connections, time-multiplexed systems require only one non-linear (spatial) node for operation. Time-multiplexing involves treating the time-varying output intensity of a single non-linear node as the output of many distinct non-linear (virtual) neurons. By sampling the non-linear device at a discrete temporal separation (referred to as θ) the output for a set number of virtual nodes (N_v) can be interpreted, realising a virtual neural network (see ref. 38 for a review on time-multiplexed photonic RC). Whilst spiking neural networks (SNNs) and reservoir computers (RCs) are typically regarded as separate concepts, the p-SNN in this work has the architecture of a so-called Extreme Learning Machine (ELM). ELMs can be understood as a specific case of RCs, but without recurrent connections (and therefore without in-built system memory), and where the information only flows in a feed-forward manner. However, as in the RC paradigm in ELMs (and thus also in the p-SNN of this work), the connections between nodes in the network are determined by the system and are not trained. In the case of the p-SNN of this work (defining as said a photonic spiking ELM), the threshold-and-fire feature of the spiking mechanism in the VCSEL is used as the activation function, whilst network connectivity is enabled by the temporal integrate-and-fire and refractory period of the spiking dynamics in the VCSEL. In particular the refractoriness in the system allows to inhibit later nodes from spiking in the p-SNN from spiking despite the direct (temporal) input to those nodes, creating longer range connections extending throughout the network. We must also note that whilst the p-SNN of this work shares with traditional spatially-extended SNNs (typically implemented with electronic hardware or in software) its use of spiking signals to process information, it differs from them in that it does not make use of many individual spatially distributed spiking neurons encoding information in the exact timings of the spikes. On the contrary, the p-SNN of this work relies on time-multiplexing approaches, allowing for an extremely hardware-friendly implementation using a single nonlinear (photonic spiking) node. In particular, this work uses a single telecom 1300 nm-VCSEL yielding a temporal high-speed non-linear spiking optical output to realise an entire p-SNN of hundreds of (virtual) spiking neurons. Figure 1a provides the experimental setup developed to implement and investigate the VCSEL-based p-SNN of this work (Methods section). Figure 1b plots a schematic diagram of the node coupling scheme and architecture of the p-SNN for its use in the chaotic time-series prediction tasks.

In our experiments, the selected individual node time was equal to $\theta = 250$ ps (approximately one quarter of the 1 ns refractory period of this VCSEL's spiking behaviour); thus, readily allowing without any further optimisation to operate at 4 GHz input data rates. Additionally, we investigated experimentally three different p-SNN sizes with total node counts of $N_v = 256, 512$ and 1024. In the p-SNN of this work, the connections between (virtual) nodes within the network are fixed and are dictated by the temporal carrier dynamics of the spiking VCSEL³⁴. Therefore, in this type of p-SNN (defining in fact a photonic spiking ELM), as in the RC paradigm, both the input and hidden layer connections are fixed and only the output layer weights require training. This allows for highly-reduced training protocols compared with fully trained networks, whilst simultaneously permitting hardware-friendly implementations and high-accuracy in key processing tasks (for a review on VCSEL-based photonic RC systems see for example³³ and references therein). The input weights mapping the feature space to the input values for each virtual node are not trained and are selected randomly from a uniform distribution between 0 and 1. This offers the same benefits as in RC systems in terms of lightweight training process. Importantly, the use of (optical) spikes to process information in the VCSEL p-SNNs of this work, has further benefits when compared to traditional non-spiking photonic neural network implementations. These include the possibility to use novel training algorithms that only require the training of very few network nodes (only in the output layer), they allow operation with sparse signalling and weight matrices, permit the use of binary (0 or 1)

Fig. 1 | Experimental layout and logical architecture of the neural network. **a** Diagram of the experimental photonic spiking neural network. A tuneable laser (TL) provides light which is intensity modulated by a Mach Zehnder (MZ) modulator. The input to the MZ modulator is given by a DC bias (generated by a Power Source, PS) and an arbitrary wave generator (AWG) followed by an RF amplifier (AMP), encoding the data to be processed into the time varying intensity of the light. Polarisation controllers (PC) are used to match the light polarisation of the input signal to that of the MZ modulator and the VCSEL. The input signal is monitored with a Power Meter (PM) and oscilloscope (OSC). The modulated light signal is then injected into the VCSEL where it can trigger ultrafast optical spikes. The VCSEL's output is read by an optical spectrum analyser (OSA) and a photodiode and oscilloscope (OSC). **b** Schematic diagram of the architecture of the VCSEL-based p-SNN^{34,35}.



weights, and they yield accurate operation even when low dataset sizes are used for training (particularly for classification tasks, as reported in refs. 34,35).

Recent works have reported the application of VCSEL-based p-SNNs to perform complex classification tasks, achieving very good performance^{34,35}. Notably, the use of ultrafast optical spikes in the p-SNN to process information, offered important additional advantages, including the ability to operate with very small training dataset sizes (down to just a few examples), the ability to tune its node count and change therefore the network architecture, and the possibility to operate with highly-efficient learning protocols requiring only the use of less than 1% of the output layer nodes for operation^{34,35}. However, to date these p-SNNs given their feed-forward architecture (without in-built recurrent connections) lack internal system memory, and therefore their use in strategic memory-requiring processing functionalities has remained elusive. The present work tackles this crucial challenge, demonstrating an induced memory technique in the p-SNN of this work to enable its successful operation in memory-requiring chaotic time-series prediction tasks, achieving high accuracy, whilst enabling hardware-friendly implementation using a single VCSEL.

Results

Time series prediction is the task of predicting a future value in a sequence of numbers in a time-series, given the preceding values. This is a highly interesting task for different key applications, such as predictive maintenance, weather forecasting, to name but a few. However, for sequences (time-series) defined by complex or chaotic dynamics, multi-step-ahead predictions can be a very challenging task, as subsequent values are not strongly correlated to previous historic values in the sequence.

Time-series prediction has been previously investigated in traditional (non-spiking) photonic reservoir computing (RC) systems, especially in photonic implementations based upon time delay reservoirs (TDRs) using semiconductor lasers, and also including VCSELs as core nonlinear elements (see for example^{32,33} and references therein). In such systems, there is an explicit optical delayed-feedback loop (typically implemented by an optical fibre link), forming recurrent connections and therefore allowing data injected in previous steps to continue circulating in the system; hence creating internal memory and influencing the output and subsequent predictions. This memory effect allows photonic TDRs to combine information from several data points in the input time series to make accurate future-value predictions³⁹⁻⁴².

However, to date VCSEL-based p-SNNs^{34,35} do not include in its structure any intrinsic mechanism to create recurrent connections, and within them the information flows in a feed-forward manner. This circumstance means that the internal system memory inherent to photonic

TDRs is not present in the VCSEL p-SNN, disabling their use for time-series prediction functionalities. We tackle this key challenge proposing an alternative data encoding approach allowing to create memory effects in the p-SNN. This is realised during the input data stage, by adding to the original data input a delayed copy of the time series. In this situation, at a given time-instant the input information contains two data input points, namely the present and a delayed value³⁶, using which the system is able to make multi-step-ahead predictions of a time-series. With this simple, yet very powerful approach, information about the long-range dynamics of the time-series to be predicted is made available to the p-SNN, thus effectively creating memory in the system. Notably, this is done without the need to add external fixed optical delay feedback lines, which increase complexity, require precise temporal control and can limit the total processing rate of the system. Importantly, the lack of external optical feedback lines in the p-SNN, also permits to drive the system in a so-called Extreme Learning Machine (ELM) configuration, with the information flowing in a feed-forward manner. This readily allows the tuning of the total number of nodes in the p-SNN, without influencing the dynamical characteristics of the nodes, simply by controlling the temporal spread of the input information^{34,35}. This permits the user to easily set diverse networks with higher or lower node counts depending on the complexity of the task to be processed by the p-SNN.

To investigate the operation of the VCSEL p-SNN for time-series prediction, we focus on demonstrating the system's ability to perform multi-step-ahead predictions of the Mackey Glass chaotic time series, defined by the delay differential equation in Eq. (1)³⁷.

$$\frac{dy}{dt} = \frac{\beta_0 y(t - \tau)}{1 + y(t - \tau)^n} - \gamma y(t) \quad (1)$$

For the experimental demonstrations of this work we used a data set of 8000 inputs and targets to demonstrate the time-series prediction functionality of the VCSEL p-SNN. Figure 2 shows the 8000 time-series point sequence used as data input. To encode the inputs of the Mackey-Glass time series for their optical injection into the VCSEL p-SNN, each given data point was combined into a two-component vector with the data point delayed by 10 steps (as shown graphically in Fig. 3). These resulting vectors were then multiplied by a randomly chosen input weight 'mask' to give the input values for each of the virtual nodes forming the p-SNN. The input mask was thus a matrix with a dimension of $2 \times N_v$, where N_v describes the total number of nodes in the network, with entries drawn uniformly at random from the interval [0,1]. The resulting masked input was then normalised so that all values were in the range [0,1] and were concatenated to generate the RF signal with the input data to be encoded optically (with the Mach-Zehnder Modulator in the setup) for injection into the 1300 nm-

Fig. 2 | The Mackey Glass time series. Time-trace showing the 8000 data points of the chaotic Mackey-Glass time-series used for the experimental investigation of the next-step ahead prediction task in the VCSEL-based p-SNN.

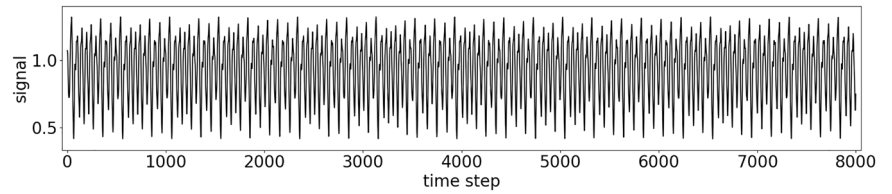


Fig. 3 | Operation of the p-SNN in the time series prediction task. The time series defined by the Mackey-Glass equations is shown in blue and dashed orange. The task is to use the values before a particular time step (in this case time-step 2810) to predict the value several steps ahead. To do this, the value at the time step and the value 10 steps preceding (both marked with green circles) are combined and processed in the p-SNN to find a prediction (represented with the purple circle). The inset provides the half of the full time-series.

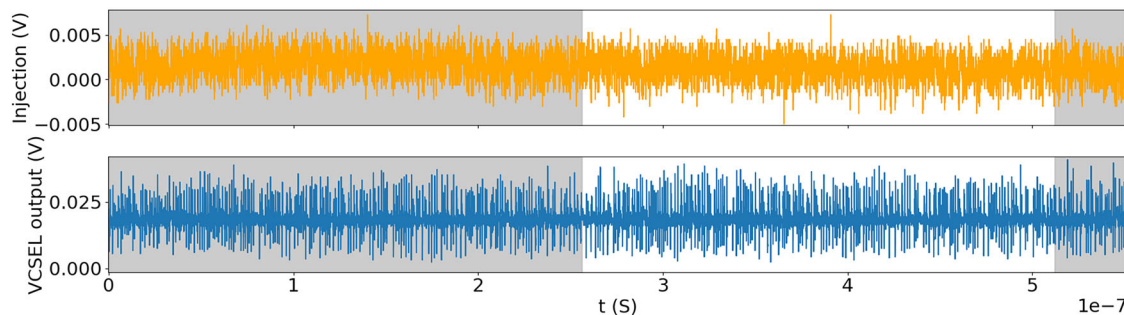
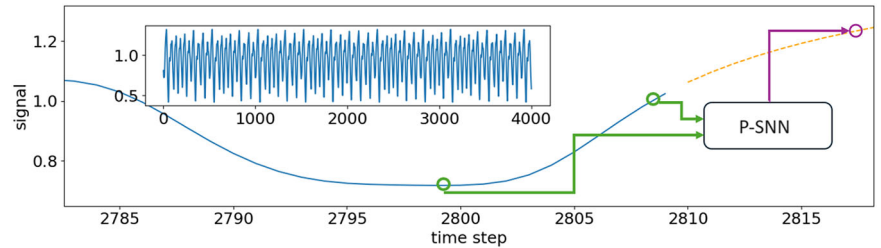


Fig. 4 | Input and output signals. Photodetector recording of the intensity of light injected and resulting intensity output from the VCSEL p-SNN showing the triggered ultrafast (sub-nanosecond long) optical spikes. The p-SNN was set here with a total node count of $N_v = 1024$; thus, giving a total processing time per point of 256 ns.

The plots show the trace for two data points of the Mackey-Glass time-series lasting from 0 ns to 256 ns (shaded region), and from 256 ns to 512 ns (unshaded region) and the achieved optical spiking outputs.

VCSEL at the core of the p-SNN. The input delay of 10 steps was chosen to enable multi-step-ahead predictions resulting in predictions horizons of about 10-time units of the Mackey-Glass system^{36,43}.

Figure 4a, b shows exemplar input and output optical signals from the VCSEL p-SNN after their temporal analysis with the high-speed photodetector and real time oscilloscope in the setup. In particular, Fig. 4a depicts the temporal varying nature of the optical input signal entering the p-SNN with the encoded Mackey-Glass data points. Figure 4b shows in turn the high-speed optical spike firing signal obtained at the output of the p-SNN in response to the input shown in Fig. 4a. For the results in Fig. 4a, b, the p-SNN was set with a node time of 250 ps and a total network node count of $N_v = 1024$; hence yielding a total processing time of 256 ns per data-point. Figure 4a, b therefore depicts the input and output signals of the p-SNN when two consecutive data input points of the Mackey-Glass time series are injected into the system.

The Mackey-Glass chaotic time series prediction task was run on the VCSEL p-SNN using three total node counts, namely $N_v = 256, 512$ and 1024, which for a set node time of 250 ps gave processing times of 64, 128 and 256 ns per data point respectively. In all cases of analysis, the 1300 nm-VCSEL at the core of the p-SNN was biased with a driving current of 3.51 mA at a temperature of 293 K³⁵, and the detuning of the injection frequency from the peak frequency of the subsidiary (orthogonally-polarised) mode of the VCSEL was -3.6 GHz. The average injection power in each case was 127 μ W, 123 μ W and 131 μ W for the p-SNN architecture set with 256, 512 and 1024 nodes, respectively. We must note

that while the average injection power differed slightly, in all cases the VCSEL was in the same dynamical regime that allowed for excitable spikes. The small specific differences were due to the variations in the randomly generated input weights and did not have a significant effect on the optical spiking dynamics (integration and refractoriness) triggered in our photonic SNN and which were used to perform the time-series prediction tasks described in this work.

To train the p-SNN to perform the chaotic Mackey-Glass time-series prediction task, the following procedure was applied: first the optical spike pattern (binary) vectors obtained from the p-SNN for all input data points used for training are collected into a state matrix. Then, the state matrix and vector of target time-series values are used to find the output layer weight matrix (a vector of length N_v) by means of least-squares regression. After the training process, during the testing phase, the binary vectors with the p-SNN's output spiking response obtained for subsequent input data points, are multiplied by the calculated output layer weight matrix, to obtain the predicted values of the Mackey-Glass chaotic time-series. This process permits to transform the binary (spiking/non-spiking) temporal output of the p-SNN into a real number providing the next-ahead predicted value.

The spike pattern vectors for the entire dataset used in this work is shown in Fig. 5, sorted according to the value that is to be predicted. Different nodes are active (i.e. contain spikes) for different ranges of the value, which is learned by the least-squares regression fitting.

The performance of the p-SNN on multi-step-ahead prediction of the Mackey-Glass chaotic time-series for prediction horizons of 1 to 15 is shown

Fig. 5 | Spiking patterns generated by the VCSEL. Temporal maps depicting the optical spike patterns delivered by the VCSEL p-SNN in response to the input data values of the Mackey-Glass time-series. Three different network architectures with total node count (N_v) of $N_v = 256$ (a, d), $N_v = 512$ (b, e) and $N_v = 1024$ (c, f) are investigated. The panels (d–f) provide zoomed in regions of the temporal maps that demonstrate differences in the optical spiking patterns achieved in different network nodes for different values of the Mackey-Glass time-series.

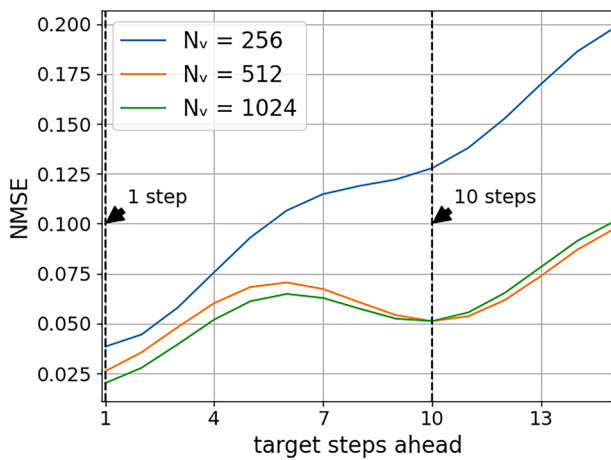
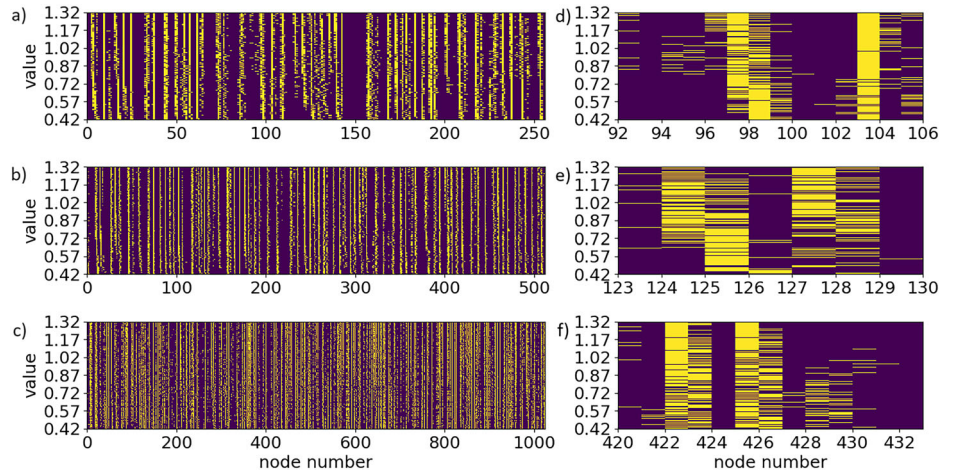


Fig. 6 | Multi-step-ahead prediction performance. Performance of the VCSEL p-SNN using input pairs comprised of the current value of the Mackey-Glass time-series and the value delayed by 10-steps for each node number (N_v) used. The x-axis is the number of steps ahead of the target and the y-axis gives the accuracy of the predictions in terms of the Normalised Mean Squared Error (NMSE). Training and testing parameters: training set size is 6000, testing set size is 1500 and the regularisation parameter is 0.03.

in Fig. 6. The accuracy of the p-SNN has been measured using the Normalised Mean Squared Error (NMSE) which is calculated using the relation provided in Eq. (2). There, the true values are denoted y and the prediction is denoted \hat{y} . Figure 6 shows that despite the lack of intrinsic hardware memory of the p-SNN and the limited temporal information provided to it, very good prediction performance is achieved over the entire prediction range. A local minimum in the prediction error is evident around 10-steps-ahead, where a low NMSE value equal to only 0.051 is achieved. This is because the input delay of 10 used in this setup, is optimised to 10-step-ahead predictions³⁶. The lowest errors are achieved for one-step-ahead predictions (with NMSE reducing to only 0.021), as the time-series values are highly correlated over this time range³⁷. We selected the NMSE metric as this has widely used to analyse accuracy in traditional photonic RC systems (including those recently reported based upon VCSELs), in chaotic time series prediction tasks^{32,33}. Hence, we also use it here to allow for a better comparison between the performance of the VCSEL p-SNN of this work with other photonic approaches.

$$NMSE = \frac{\sum_i (y_i - \hat{y}_i)^2}{\sigma_y^2} \quad (2)$$

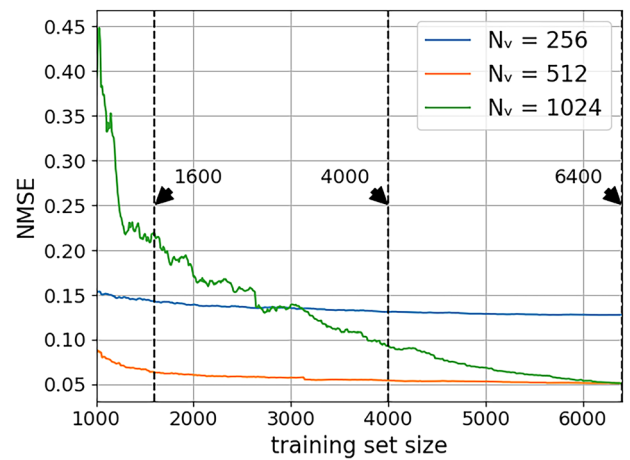


Fig. 7 | Performance against Training set size. Performance of the VCSEL p-SNN in the 10-step-ahead prediction of the Mackey-Glass time-series as a function of the training data set size, for each node number (N_v) used. The prediction error is the Normalised Mean Squared error (NMSE). Training and testing parameters: testing set size is 1500 and the regularisation parameter is 0.03.

Recent works have outlined that p-SNNs, thanks to their use of spikes to process information, offer very good performance in classification tasks, even when highly reduced training dataset sizes are used³⁵. This provides an advantage when compared with traditional photonic RC implementations, which typically require larger dataset sizes during the training phase to achieve good accuracy across complex tasks. Following on these recent promising reports in p-SNNs^{34,35}, in this work we have analysed the effect of the training data set size in the VCSEL p-SNNs performance on the Mackey-Glass time-series prediction task. Figure 7 shows the influence of the training data set size for 10-step-ahead predictions. Here we find very good performance for training sets as small as 1600 datapoints (20% of total data points applied to the system) using the p-SNN with a 512-node network architecture. Figure 7 also shows that for a larger network node count of 1024 nodes, larger training sets are needed to avoid overfitting.

To highlight the system operation, detailed results are provided in this work for three different training data sizes, namely 1600, 4000 and 6400 points (20%, 50% and 80% of total), and for the three different network architectures (with 256, 512 and 1024 nodes) investigated. Figure 8 plots as an example of the VCSEL p-SNN performance in the Mackey-Glass time series prediction task for both 10 steps-ahead (Fig. 8a) and 1 step-ahead (Fig. 8b) predictions. For the results in Fig. 8a, b, a dataset formed by the first time-ordered 4000 points (50% of the total 8000 points applied) in the time-

Fig. 8 | Examples of time series prediction. Performance of the p-SNN in the prediction of step-ahead values of the Mackey-Glass time series using a network with 512 virtual nodes and applying a training dataset using 4000 points (50% of total). **a, b** Predicting 10 steps ahead. **c, d** Predicting the next step ahead. **a, c** Predicted (orange) and true (blue) time-series values, with the first 4000 points shown in blue providing the training dataset. The inset in plots (a) and (c) shows a zoomed in region between data points 6500 and 6700 of the Mackey-Glass time-series showcasing in more detail the good system performance in this prediction task. **b, d** Correlation between true and predicted values (in red is shown the line where prediction = truth).

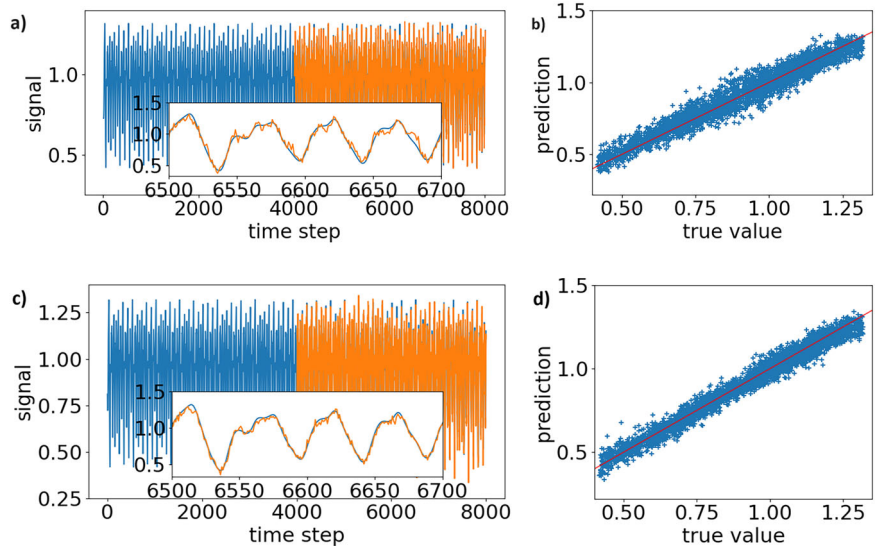


Table 1 | Error and correlation against training set size

Node count	Training set %	NMSE	Correlation
	20	0.148	0.91
256	50	0.134	0.92
	80	0.131	0.92
	20	0.066	0.97
512	50	0.055	0.97
	80	0.051	0.97
	20	0.213	0.87
1024	50	0.087	0.95
	80	0.051	0.97

Experimentally obtained values of NMSE (Normalised Mean Square Error) and correlation coefficient for 10-steps ahead predictions for three different configured network node architectures in the p-SNN and different training set sizes (as a percentage of 8000).

series is used for the training phase, and the last 4000 points are used during inference. For the specific cases investigated in Fig. 8 the p-SNN was configured with a total node count of 512 nodes, which at 250 ps/node, yields a total processing time of 128 ns per data point. The blue and orange traces in Fig. 8a, b plot respectively the original time-series and the predicted values delivered by the p-SNN. Figure 8a, b shows that very good performance is obtained in both the 10 and 1 steps-ahead prediction tasks with the p-SNN. This is further illustrated in the insets in Fig. 8a, b showing in detail different smaller temporal sequences, highlighting the high-accuracy performance in the time-series prediction task delivered by the p-SNN, even when a very small dataset set (50% of total points) is utilised for training and with all data points fed in a timely-ordered manner.

The accuracy of the p-SNN has also been measured using the correlation between true and predicted values. To that end we calculated the Pearson correlation coefficient using Eq. (3). There, the true values are denoted y and the prediction is denoted \hat{y} . This measures how well the predictions depend linearly on the true value (a Pearson coefficient of 1.0 implies perfect linearity between the two variables). The plots at the right side of Fig. 8a, b provide the correlation between true and predicted values for the two examples considered, further highlighting the good performance of the system in predicting different step-ahead values of the Mackey-Glass time-series. A full set of experimental results on this chaotic time-series prediction task obtained for the selected training dataset sizes, 20%, 50% and 80%, and for the network architectures with 256, 512 and 1024 nodes are

provided in the supporting information accompanying this article. In all cases investigated, for all cases of training data set sizes and network node count, the results highlight the successful, high-accuracy performance of the p-SNN in the chaotic time series prediction task investigated in this work.

$$\rho = \frac{\text{cov}(y, \hat{y})}{\sigma_y \sigma_{\hat{y}}} \quad (3)$$

Table 1 shows the performance of the p-SNN in the 10 steps-ahead value prediction of the chaotic Mackey-Glass time series, measured from the calculated NMSE and correlation coefficients for the 3 specific cases of training dataset sizes of 20%, 50% and 80% (as percentage of the 8000 points used) and for network architectures with $N_v = 256$ (see Supplementary Figs. 1–3), 512 (Supplementary Figs. 4–6) and 1024 nodes (Supplementary Figs. 7–9), investigated in this work. The results in Table 1 highlights that for all cases of analysis high-accuracy is found in the 10 steps-ahead prediction of the Mackey-Glass time-series, as per the small obtained values of NMSE (as low as NMSE = 0.051, when $N_v = 512$) and high levels of correlation (up to 0.97 is achieved in multiple cases of analysis) between true and prediction values.

While the performance of this p-SNN is comparable to that of typical photonic reservoir computing platforms^{23,32}, the distinct lack of a fixed length optical feedback loop reduces hardware complexity and allows arbitrarily changing the number of nodes used by the p-SNN at will, allowing improved performance in exchange for processing speed (or vice versa) as desired. It must be noted that only the output weight matrix is trained in this process, and the input weights are chosen randomly. The use of spikes also offers potential advantages over continuous value reservoir computers such as binary output weights and simplified training algorithms³⁵.

Conclusion

This work reports experimentally the successful operation of a VCSEL-based photonic Spiking Neural Network (p-SNN) on complex time-series prediction tasks. Specifically, we demonstrate the system’s accurate performance on multi-step-ahead predictions of the chaotic Mackey-Glass time series. Our results reveal that the p-SNN of this work offers excellent performance yielding high prediction accuracy whilst benefitting from ultrafast and efficient operation (~120 μW avg. optical input power, and ~3.5 mA bias current requirements) as well as from a highly hardware-friendly and inexpensive implementation using a single telecom-wavelength VCSEL and commercially-sourced telecom components. The VCSEL p-SNN of this work uses time-multiplexing to create a feed-forward network, with connectivity between neighbouring (virtual) optical spiking nodes, and the

nonlinear network responses provided by the VCSEL's ultrafast neural-like excitability, its leaky-integrate and fire optical spiking dynamics, alongside the inhibitory effects induced by the refractoriness of spiking in the VCSEL. Training of the p-SNN is done only on the output layer weights, and the network operates with fixed (random) weights used in the input and hidden layers; hence reducing computational complexity while retaining highly accurate performance. Notably, our approach also eliminates the need of fixed optical delayed feedback loops to induce network recurrent connectivity and the memory needed to perform on time-series prediction tasks. Instead, a method is introduced for creating memory in the p-SNN by combining in the input data signals delayed copies of the time series; to allow past and current information to combine in the network to arrive to a successful step-ahead prediction. This is similar to typical approaches using feedforward networks or non-linear vector regression. However, here we have demonstrated a minimal approach by using only one additional time-delayed version of the input timeseries. Due to the lack of recurrent connectivity of the p-SNN the number of nodes in the network can be freely tuned as needed, without requiring any hardware modifications or controls. This permits the p-SNN to offer additional flexibility to optimise for prediction accuracy or computation speed. Moreover, the use of optical spikes to process information in the p-SNN offers inherent advantages, such as the direct use of optical spiking patterns (rather than continuous signals) to distinguish between different time-series values and accurate operation with very small training data set sizes. We demonstrate that our VCSEL-based p-SNN offers high accuracy operation (down to NMSE values as low as 0.051 for a prediction horizon of 10-steps-ahead are demonstrated experimentally) in the Mackey-Glass chaotic multi-step-ahead prediction.

Methods

Experimental setup

The Photonic Spiking Neural Network (p-SNN) of this work is built using the experimental setup shown in Fig. 1. At its core, the p-SNN employs a single telecom-wavelength 1300nm-VCSEL as a non-linear element for the transformation of light-encoded input data information into fast optical (neuronal) spiking signals. Standard fibre-optic telecom components are used in the setup to control, inject and analyse the system's optical signals, keeping this p-SNN approach hardware-friendly, affordable, and fully-compatible with optical communication networking and data-centre technologies. The widely employed technique of optical injection is used to introduce the input data information into the VCSEL-based p-SNN. In the optical injection arm of the setup, Continuous Wave (CW) light produced by a 1300 nm tuneable laser (TL) source is intensity modulated using a 10 Gbps Mach-Zehnder (MZ) Modulator. A Power Source (PS) generates the DC bias voltage applied to the MZ Modulator, whilst a 12 Gsa/s, 5 GHz-bandwidth Arbitrary Wave Generator (AWG) coupled to an RF amplifier (AMP), is used to drive the MZ Modulator with an RF signal providing the encoded input information. The optical signal in the injection arm is split by a 50:50 fibre-optic directional coupler. A first output is connected to an optical power meter to monitor the optical injection strength, whilst the second branch is split again by a 99:1 coupler. The low power (1%) branch is used to read the optical injection, and the second branch is connected to an optical circulator. The latter is used to inject the optical input signal into the 1300nm-VCSEL as well as to capture its optical output signal for subsequent analysis. The polarisation of the injected light is set using fibre polarisation controllers (PC) to ensure maximal coupling into the MZ Modulator and the VCSEL. Signal analysis was performed using a 9 GHz amplified photodetector, a 40 Gsa/s, 16 GHz-bandwidth real-time Oscilloscope (OSC) and an Optical Spectrum Analyser (OSA). At room temperature ($T = 293$ K) the threshold current of the VCSEL measured 1.4 mA, and when operated at the selected bias current of 3.51 mA, the device produced fundamental mode emission with two orthogonally-polarised peaks at 1287.65 nm and 1287.506 nm (see ref. 35 for details on the LI curve and optical spectrum of the VCSEL). These correspond to the two orthogonal polarisations of the fundamental transverse mode of the device. Injection was made into the subsidiary mode (at 1287.668 nm) with mode-matched

polarisation and a frequency detuning of -3.2 GHz. An average optical injection power of ~ 120 μ W was incident on the VCSEL, which when run in the absence of modulation, achieved the injection locking of the device to the external signal from the TL⁴⁴. Fast modulation of the injection signal around these injection conditions induced fast (sub-nanosecond) optical (neural-like) spiking responses, key to the operation of the system as a p-SNN^{34,35}.

Mackey-glass timeseries

The Mackey-Glass equations were numerically integrated using a fourth order Runge-Kutta method with Hermitian interpolation for the delayed mid-steps. The integration time step was 0.01. The timeseries was then down-sampled to time steps of 1.

Training and testing

The p-SNN was trained using least-squares regression. Using this method, the weights for each node were calculated using Eq. (4).

$$W_{out} = (S^T S + \lambda I)^{-1} S^T y \quad (4)$$

Where the matrix S is formed of the optical spiking output of the VCSEL for each data point arranged row wise, where a node containing a spike is denoted by a one, and a node without a spike by a zero. The vector y is the (column) vector of corresponding output values that the p-SNN should predict. The regularisation parameter λ was chosen to minimize the NMSE.

Data availability

All data underpinning this publication are openly available from the University of Strathclyde KnowledgeBase at <https://doi.org/10.15129/7350af10-809d-4c5d-b41b-0951f31e7f6c>.

Received: 8 May 2024; Accepted: 11 February 2025;

Published online: 20 March 2025

References

- Frady, E. P. et al. Efficient Neuromorphic Signal Processing with Resonator Neurons. *J. Signal Processing Syst.* **94**, 917–927 (2022).
- DeBole, M.V. et al. TrueNorth: Accelerating From Zero to 64 Million Neurons in 10 Years. *Computer*, **52**, 20–29 (2019).
- Höppner, S. et al. The SpiNNaker 2 Processing Element Architecture for Hybrid Digital Neuromorphic Computing. Preprint at <http://arxiv.org/abs/2103.08392> (2021).
- Pehle, C. et al. The BrainScaleS-2 Accelerated Neuromorphic System With Hybrid Plasticity. *Front. Neurosci.* **16**, <https://doi.org/10.3389/fnins.2022.795876> (2022).
- Schuman, C.D. et al. Opportunities for neuromorphic computing algorithms and applications. *Nat. Comput. Sci.* **2**, 10–19 (2022).
- Christensen, D. V. et al. 2022 roadmap on neuromorphic computing and engineering. *Neuromorphic Comput. Eng.* **2**, 022501 (2022).
- Zhang, H. et al. An optical neural chip for implementing complex-valued neural network. *Nat. Commun.* **12**, 457 (2021).
- de Lima, T. F. et al. Noise Analysis of Photonic Modulator Neurons. *IEEE J. Sel. Topics Quantum Electronics*, **26**, 1–9 (2020).
- Feldmann, J., Youngblood, N., Wright, C. D., Bhaskaran, H. & Pernice, W. H. P. All-optical spiking neurosynaptic networks with self-learning capabilities. *Nature* **569**, 208–214 (2019).
- Pammi, V. A., Alfaro-Bittner, K., Clerc, M. G. & Barbay, S. "Photonic Computing With Single and Coupled Spiking Micropillar Lasers,". *IEEE J. Sel. Top. Quantum Electron.* **26**, 1–7 (2020).
- Chen, Z. et al. Deep learning with coherent VCSEL neural networks. *Nature Photonics* **17**, 723–730 (2023).
- Hurtado, A. & Javaloyes, J. Controllable spiking patterns in long-wavelength vertical cavity surface emitting lasers for neuromorphic photonic systems. *Appl. Phys. Lett.* **107**, 241103 (2015).
- Robertson, J., Wade, E., Kopp, Y., Bueno, J., & Hurtado, A. Towards Neuromorphic Photonic Networks of Ultrafast Spiking Laser Neurons.

- IEEE J. Selected Top. Quantum Electronics*, <https://doi.org/10.1109/JSTQE.2019.2931215> (2019).
14. Robertson, J., Hejda, M., Bueno, J., & Hurtado, A. Ultrafast optical integration and pattern classification for neuromorphic photonics based on spiking VCSEL neurons. *Sci. Rep.* **10**, <https://doi.org/10.1038/s41598-020-62945-5> (2020).
 15. Hejda, M., Robertson, J., Bueno, J., & Hurtado, A. Spike-based information encoding in vertical cavity surface emitting lasers for neuromorphic photonic systems. *J. Phys. Photonics*, **2**, 44001 (2020).
 16. Zhang, Y. et al. Experimental demonstration of pyramidal neuron-like dynamics dominated by dendritic action potentials based on a VCSEL for all-optical XOR classification task. *Photonics Res.* **9**, 1055 (2021).
 17. Robertson, J. et al. Image edge detection with a photonic spiking VCSEL-neuron. *Optics Express* **28**, 37526–37537 (2020).
 18. Zhang, Y. et al. All-optical neuromorphic binary convolution with a spiking VCSEL neuron for image gradient magnitudes. *Photon. Res.* **9**, B201–B209 (2021).
 19. Robertson, J. et al. Image edge detection with a photonic spiking VCSEL-neuron. *Optics Express*, **28**, 37526–37537 (2020).
 20. Hejda, M., Robertson, J., Bueno, J., Alanis, J. A. & Hurtado, A. Neuromorphic encoding of image pixel data into rate-coded optical spike trains with a photonic VCSEL-neuron. *APL Photonics* **6**, 60802 (2021).
 21. Appeltant, L. et al. Information processing using a single dynamical node as complex system. *Nat. Commun.* **2**, 468 (2011).
 22. Borghi, M., Biasi, S., & Pavesi, L. Reservoir computing based on a silicon microring and time multiplexing for binary and analog operations. *Sci. Rep.* **11**, 15642 (2021).
 23. Donati, G., Mirasso, C. R., Mancinelli, M., Pavesi, L., & Argyris, A. Microring resonators with external optical feedback for time delay reservoir computing. *Optics Express*, **30**, 522 (2022).
 24. Castro, B. J. G., Peucheret, C., Zibar, D., & Da Ros, F. Effects of cavity nonlinearities and linear losses on silicon microring-based reservoir computing. <https://doi.org/10.48550/arXiv.2310.09433> (2023).
 25. Takano, K. et al. Compact reservoir computing with a photonic integrated circuit. *Optics Express*, **26**, 29424 (2018).
 26. Nakajima, M., Tanaka, K., & Hashimoto, T., Scalable reservoir computing on coherent linear photonic processor. *Commun. Phys.* **4**, 20 (2021).
 27. Vatin, J., Rontani, D., & Sciamanna, M. Enhanced performance of a reservoir computer using polarization dynamics in VCSELs. *Optics Lett.* **43**, 4497 (2018).
 28. Huang, Y., Zhou, P., Yang, Y. G., Cai, D. Y. & Li, N. Q. Enhanced performance of reservoir computing using multiple self-injection and mutual injection vcsels. *IEEE J. Sel. Top. Quantum Electron.* **29**, 1–9 (2023).
 29. Porte, X. et al. A complete, parallel and autonomous photonic neural network in a semiconductor multimode laser. *J. Phys.* **3**, 024017 (2021).
 30. Skalli, A. et al. Computational metrics and parameters of an injection-locked large area semiconductor laser for neural network computing. *Opt. Mater. Express* **12**, 2793–2804 (2022).
 31. Vatin, J., Rontani, D., & Sciamanna, M. Experimental realization of dual task processing with a photonic reservoir computer. *APL Photonics*, **5**, 086105 (2020).
 32. Bueno, J., Robertson, J., Hejda, M. & Hurtado, A. “Comprehensive Performance Analysis of a VCSEL-Based Photonic Reservoir Computer,”. *IEEE Photonics Technol. Lett.* **33**, 920–923 (2021).
 33. Skalli, A. et al. Photonic neuromorphic computing using vertical cavity semiconductor lasers. *Optical Mater. Express*, **12**, 2395 (2022).
 34. Owen-Newns, D., Robertson, J., Hejda, M., & Hurtado, A., Ghz rate neuromorphic photonic spiking neural network with a single vertical-cavity surface-emitting laser (vcSEL). *IEEE J. Selected Topics Quantum Electronics*, **29**, 1–10 (2023).
 35. Owen-Newns, D., Robertson, J., Hejda, M., & Hurtado, A., Photonic spiking neural networks with highly efficient training protocols for ultrafast neuromorphic computing systems. *Intelligent Comput.* **2**, 0031 (2023).
 36. Jaurigue, L., Robertson, E., Wolters, J., & Lüdge, K., Reservoir Computing with Delayed Input for Fast and Easy Optimisation. *Entropy*, **23**, 1560 (2021).
 37. Mackey, M. C. & Glass, L. Oscillations and Chaos in physiological control systems. *Science* **197**, 287–289 (1977).
 38. Hülser, T., Köster, F., Jaurigue, L., & Lüdge, K., Role of delay-times in delay-based photonic reservoir computing. *Optical Mater. Express*, **12**, 1214 (2022).
 39. Freiburger, M. et al. Improving time series recognition and prediction with networks and ensembles of passive photonic reservoirs. *IEEE J. Sel. Top. Quantum Electron.* **26**, 1–11 (2020).
 40. Cai, D., Huang, Y., Yang, Y., Zhou, P. & Li, N. Enhanced performances of photonic reservoir computing using a semiconductor laser with random distributed optical feedback. *Opt. Lett.* **48**, 6392–6395 (2023).
 41. Gauthier, D. J., Erik, B., Griffith, A., & Wendson, A. S. B. Next generation reservoir computing. *Nat. Commun.* **12**, 5564 (2021).
 42. Hülser, T., Köster, F., Lüdge, K., & Jaurigue, L. Deriving task specific performance from the information processing capacity of a reservoir computer. *Nanophotonics* **12**, 937–947 (2023).
 43. Jaurigue, L. C. & Lüdge, K. Reducing reservoir computer hyperparameter dependence by external timescale tailoring. *Neuromorph. Comput. Eng.* **4**, 014001 (2024).
 44. Nizette, M., Sciamanna, M., Gatara, I., Thienpont, H. & Panajotov, K. Dynamics of vertical-cavity surface-emitting lasers with optical injection: a two-mode model approach. *J. Opt. Soc. Am. B* **26**, 1603–1613 (2009).

Acknowledgements

The authors acknowledge this work was supported by the UKRI Turing AI Acceleration Fellowships Programme (EP/V025198/1), and by the EU Pathfinder Open project ‘SpikePro’. The authors acknowledge support from the Fraunhofer Centre for Applied Photonics, FCAP.

Author contributions

D.O.-N., A.A. and J.R. carried out the experimental analyses. J.R. and A.H. supervised the experimental activities. L.J. and K.L. contributed the memory-induced technique in the network for use in time-series prediction tasks. D.O.-N implemented the training algorithms and network memory technique. D.O.-N processed the data in collaboration with A.A, J.R and J.A.J. K.L and A.H. supervised this work. All authors contributed to the writing and discussion of this manuscript.

Competing interests

The authors declare no competing interests.

Additional information

Supplementary information The online version contains supplementary material available at <https://doi.org/10.1038/s42005-025-02000-9>.

Correspondence and requests for materials should be addressed to Dafydd Owen-Newns.

Peer review information *Communications Physics* thanks the anonymous reviewers for their contribution to the peer review of this work. A peer review file is available.

Reprints and permissions information is available at <http://www.nature.com/reprints>

Publisher’s note Springer Nature remains neutral with regard to jurisdictional claims in published maps and institutional affiliations.

Open Access This article is licensed under a Creative Commons Attribution 4.0 International License, which permits use, sharing, adaptation, distribution and reproduction in any medium or format, as long as you give appropriate credit to the original author(s) and the source, provide a link to the Creative Commons licence, and indicate if changes were made. The images or other third party material in this article are included in the article's Creative Commons licence, unless indicated otherwise in a credit line to the material. If material is not included in the article's Creative Commons licence and your intended use is not permitted by statutory regulation or exceeds the permitted use, you will need to obtain permission directly from the copyright holder. To view a copy of this licence, visit <http://creativecommons.org/licenses/by/4.0/>.

© The Author(s) 2025